Electrically pumped sub-wavelength metallo-dielectric pedestal pillar lasers

Jin Hyoung Lee,[1,2] Mercedeh Khajavikhan,[1] Aleksandar Simic,[1] Qing Gu,[1] Olesya Bondarenko,[1] Boris Slutsky,[1] Maziar P. Nezhad,[1] and Yeshaiahu Fainman[1,*]

[1]*Department of Electrical and Computer Engineering, University of California at San Diego, La Jolla, California 92093, USA*

[2]*Currently with Oracle Labs, 9515 Towne Centre Drive, San Diego, California 92121, USA*

**fainman@eng.ucsd.edu*

Abstract: Electrically driven subwavelength scale metallo-dielectric pedestal pillar lasers are designed and experimentally demonstrated. The metallo-dielectric cavity significantly enhances the quality factor (Q > 1500) of the wavelength and subwavelength scale lasers and the pedestal structure significantly reduces the threshold gain (< 400 cm^{-1}) which can potentially enable laser operation at room temperature. We observed continuous wave lasing in 750 nm gain core radius laser at temperatures between 77 K and 140 K with a threshold current of 50 μA (at 77 K). We also observed lasing from a 355 nm gain core radius laser at temperatures between 77 K and 100 K.

OCIS codes: (140.3948) Microcavity devices; (140.5960) Semiconductor lasers.

References and links

1. S. L. McCall, A. F. J. Levi, R. E. Slusher, S. J. Pearton, and R. A. Logan, "Whispering-gallery mode microdisk lasers," Appl. Phys. Lett. **60**(3), 289 (1992).
2. A. F. J. Levi, "Microdisk lasers," Solid-State Electron. **37**(4-6), 1297–1302 (1994).
3. O. Painter, R. K. Lee, A. Scherer, A. Yariv, J. D. O'Brien, P. D. Dapkus, and I. Kim, "Two-dimensional photonic band-gap defect mode laser," Science **284**(5421), 1819–1821 (1999).
4. H.-G. Park, S.-H. Kim, S.-H. Kwon, Y.-G. Ju, J.-K. Yang, J.-H. Baek, S.-B. Kim, and Y.-H. Lee, "Electrically driven single-cell photonic crystal laser," Science **305**(5689), 1444–1447 (2004).
5. R. F. Oulton, V. J. Sorger, T. Zentgraf, R.-M. Ma, C. Gladden, L. Dai, G. Bartal, and X. Zhang, "Plasmon lasers at deep subwavelength scale," Nature **461**(7264), 629–632 (2009).
6. R. Perahia, T. P. Mayer Alegre, A. H. Safavi-Naeini, and O. Painter, "Surface-plasmon mode hybridization in subwavelength microdisk lasers," Appl. Phys. Lett. **95**(20), 201114 (2009).
7. S. H. Kwon, J. H. Kang, C. Seassal, S. K. Kim, P. Regreny, Y. H. Lee, C. M. Lieber, and H. G. Park, "Subwavelength plasmonic lasing from a semiconductor nanodisk with silver nanopan cavity," Nano Lett. **10**(9), 3679–3683 (2010).
8. M. W. Kim and P.-C. Ku, "Semiconductor nanoring lasers," Appl. Phys. Lett. **98**(20), 201105 (2011).
9. M. T. Hill, Y.-S. Oei, B. Smalbrugge, Y. Zhu, T. de Vries, P. J. van Veldhoven, F. W. M. van Otten, T. J. Eijkemans, J. P. Turkiewicz, H. de Waardt, E. J. Geluk, S.-H. Kwon, Y.-H. Lee, R. Nötzel, and M. K. Smit, "Lasing in metallic-coated nanocavities," Nat. Photonics **1**(10), 589–594 (2007).
10. M. A. Noginov, G. Zhu, A. M. Belgrave, R. Bakker, V. M. Shalaev, E. E. Narimanov, S. Stout, E. Herz, T. Suteewong, and U. Wiesner, "Demonstration of a spaser-based nanolaser," Nature **460**(7259), 1110–1112 (2009).
11. M. P. Nezhad, A. Simic, O. Bondarenko, B. Slutsky, A. Mizrahi, L. Feng, V. Lomakin, and Y. Fainman, "Room-temperature subwavelength metallo-dielectric lasers," Nat. Photonics **4**(6), 395–399 (2010).
12. K. Yu, A. Lakhani, and M. C. Wu, "Subwavelength metal-optic semiconductor nanopatch lasers," Opt. Express **18**(9), 8790–8799 (2010).
13. D. A. Miller, "Optical Interconnects to Silicon," IEEE J. Sel. Top. Quantum Electron. **6**(6), 1312–1317 (2000).
14. E. Purcell, "Spontaneous emission probabilities at radio frequencies," Phys. Rev. **69**, 681 (1946).
15. M. T. Hill, M. Marell, E. S. P. Leong, B. Smalbrugge, Y. Zhu, M. Sun, P. J. van Veldhoven, E. J. Geluk, F. Karouta, Y.-S. Oei, R. Nötzel, C.-Z. Ning, and M. K. Smit, "Lasing in metal-insulator-metal sub-wavelength plasmonic waveguides," Opt. Express **17**(13), 11107–11112 (2009).
16. A. Mizrahi, V. Lomakin, B. A. Slutsky, M. P. Nezhad, L. Feng, and Y. Fainman, "Low threshold gain metal coated laser nanoresonators," Opt. Lett. **33**(11), 1261–1263 (2008).
17. P. B. Johnson and R. W. Christy, "Optical Constants of the Noble Metals," Phys. Rev. B **6**(12), 4370–4379 (1972).

#149547 - $15.00 USD Received 20 Jun 2011; revised 9 Sep 2011; accepted 30 Sep 2011; published 18 Oct 2011

18. T. Baba, “Photonic crystals and microdisk cavities based on GaInAsP-InP system,” IEEE J. Sel. Top. Quantum Electron. **3**(3), 808–830 (1997).
19. T. Baba, M. Fujita, A. Sakai, M. Kihara, and R. Watanabe, “Lasing characteristics of GaInAsP-InP strained quantum-well microdisk injection lasers with diameter of 2-10 µm,” IEEE Photon. Technol. Lett. **9**(7), 878–880 (1997).
20. M. Asada and Y. Suematsu, “Density-matrix theory of semiconductor lasers with relaxation broadening model-gain and gain-suppresion in semiconductor lasers,” IEEE J. Quantum Electron. **21**(5), 434–442 (1985).
21. Z. Liu, J. M. Shainline, G. E. Fernandes, J. Xu, J. Chen, and C. F. Gmachl, “Continuous-wave subwavelength microdisk lasers at $\lambda = 1.53$ µm,” Opt. Express **18**(18), 19242–19248 (2010).
22. J. Van Campenhout, P. Rojo-Romeo, D. Van Thourhout, C. Seassal, P. Regreny, L. Di Cioccio, J.-M. Fedeli, and R. Baets, “Thermal characterization of electrically injected thin-film InGaAsP microdisk lasers on Si,” J. Lightwave Technol. **25**(6), 1543–1548 (2007).
23. F. Albert, T. Braun, T. Heindel, C. Schneider, S. Reitzenstein, S. Höfling, L. Worschech, and A. Forchel, “Whispering gallery mode lasing in electrically driven quantum dot micropillars,” Appl. Phys. Lett. **97**(10), 101108 (2010).

1. Introduction

Demonstrating the smallest possible laser structure has been of great interest not only for fundamental science but as a practical component for highly integrated photonic circuits [1–12]. Minimizing the footprint of an optical device allows a dense integration in the optoelectronic circuit and higher efficiency in energy consumption [13]. In addition, reducing the laser size can result in the modification of the spontaneous emission rate through the Purcell effect [11,14]. During the past two decades, remarkable progress in minimizing lasers to micro and nano-scale has been reported. There have been successful demonstration of reducing the laser size in one or two dimensions in the form of micro-disks [1,2] and photonic crystals [3,4]. However, the realization of the subwavelength cavity structure in all three dimensions has been challenging. The challenge comes from achieving the efficient confinement of the optical mode in all three dimensions inside the subwavelength cavity without severe radiation loss. Hybrid plasmonic mode lasers have been demonstrated in the form of nano-wire [5], nano-disk [6,7], and nano-ring [8]. However, the high optical loss associated with the plasmonic cavity was compensated by a cryogenic cooling and only the optical pumping configuration was demonstrated. Hill et al. reported a metallic subwavelength nano-pillar laser which opened a new route to creating electrically driven subwavelength-scale 3D cavities [9]. The high aspect ratio of the pillar structure and gold coated cavity form a highly confined mode in the gain core. However, the high mode overlap with the metal coating and the high ohmic loss in the metal at optical frequencies also limited the laser operation only to cryogenic environment. Room temperature operation was reported when one of the cavity dimensions was expanded to a few wavelengths and gold was substituted with silver [15]. Recently, we reported optically pumped subwavelength metallo-dielectric cavity lasers operating at room temperature, which was achieved by optimizing the cavity design [11]. The high index contrast in the vertical direction between the semiconductor gain core (InGaAsP MQW) and low refractive index claddings (air and SiO_2) strongly enhanced the vertical mode confinement. The high reflectivity of the metal allowed for efficient mode confinement while a thin low refractive index dielectric shield (SiO_2) between the gain and metal coating layer minimized the optical mode overlap with the metal coating [16]. As a result, the threshold gain was significantly reduced, enabling lasing at room temperature. However, it is always desirable to have the optical device operated by the electrical injection which allows chip-level integration with existing electronic circuitry.

In this paper we present electrically pumped metallo-dielectric subwavelength pedestal pillar lasers. Our cavity designs predict high Q factors and low threshold gains and have the potential to operate at room temperature. Experimentally, we demonstrate electrically pumped subwavelength scale laser structures with metal coatings and optimized dielectric shields. We also investigate the dependence of the lasing characteristics of our devices on temperature and size.

#149547 - $15.00 USD Received 20 Jun 2011; revised 9 Sep 2011; accepted 30 Sep 2011; published 18 Oct 2011

2. Cavity design and modeling

The platform for our devices is based on an InGaAs/InP double heterostructure grown on an InP substrate similar to the structure reported in [9]. The schematic of the laser structure is shown in Fig. 1(a). The intrinsic 300 nm thick (h_{core}) InGaAs bulk layer is the active layer and the upper (470 nm thick) and lower (450 nm thick) InP layers are the cladding layers through which the injected carriers are flowing into the active layer. Highly doped n-InGaAs on the top and p-InGaAsP in the lower cladding layer form the n and p contact layers, respectively. The top and bottom InP cladding width is intentionally reduced using selective wet etching to form a pedestal structure for enhancing the vertical optical confinement. Thin dielectric and metal layers are coated on the pillar structure which forms a metallo-dielectric cavity. We have previously reported that the metallo-dielectric cavity is able to achieve efficient lateral mode confinement in the subwavelength scale due to the high reflectivity of the metal while reducing the optical ohmic loss by minimizing the mode overlap with the metal using a thin dielectric shield [11,16]. COMSOL multiphysics was used for 3D FEM modeling of our structure. The dielectric constant of bulk silver at room temperature ($\varepsilon_{Ag} = -120.43-i3.073$ at 1.55 μm) was used for the metal coating [17]. We first designed the wavelength scale cavity in which the gain core radius (r_{core}) is 750 nm ($2r_{core} \sim \lambda$), the cladding radius (r_{clad}) is 690 nm (Δr = 60 nm) and SiO_2 shield thickness (d_{shield}) is 150 nm. The electric field intensity of the resonant cavity mode was calculated and the field intensity (horizontal cross-section) in the gain medium is shown in Fig. 1(b). The whispering gallery mode (WGM) with the azimuthal mode number (M) of 7 is supported and the electric field is strongly confined inside the metal cavity (TE mode). The thin active layer (h_{core} = 300 nm) allows only the lowest order mode in the vertical direction. The mode overlap with the metal coating is minimized by the dielectric shield as shown in Fig. 1(b). As the dielectric shield becomes thinner, the field penetration into the metal coating is increased which results in a higher loss. In contrast, a thick dielectric shield could reduce the field penetration into the metal, however, the relative ratio of gain in the whole structure is decreased which eventually results in a lower gain. Therefore, there should be an optimum thickness of the dielectric shield for given gain core radius. Details of the optimization of the dielectric shield thickness were discussed in our previous work [16].

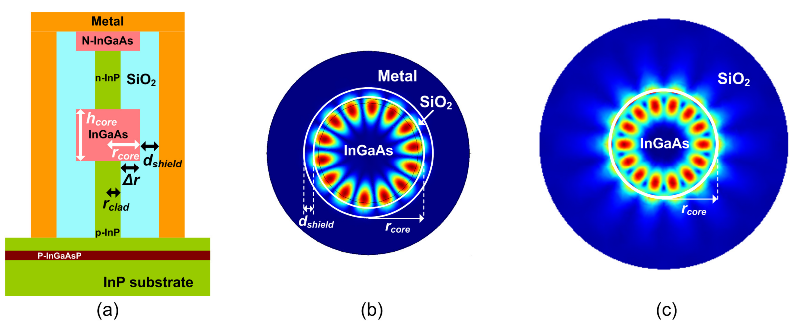

Fig. 1. A schematic of subwavelength pedestal pillar laser shown in (a) where r_{core} is the radius of InGaAs gain layer, r_{clad} is the radius of InP cladding. Δr is the difference between r_{core} and r_{clad}. d_{shield} is the thickness of SiO_2 shield layer. h_{core} is the height of InGaAs gain medium. (b) The horizontal cross section of the electric field intensity when r_{core} = 750 nm, r_{clad} = 690 nm (Δr = 60 nm), and d_{shield} = 150 nm with silver coating. (c) The horizontal cross section of the electric field intensity in the same structure with only low index dielectric (SiO_2) coating. r_{core} in (b) and (c) are the same as 750 nm.

For comparison, we numerically modeled the same pedestal structure coated only by a low index dielectric (n_{SiO2} = 1.45) without a metal coating. The electric field intensity of the resonant mode of this dielectric cavity is shown in Fig. 1(c). It shows significant mode spreading outside the gain medium which results in low mode overlap with the gain medium. In our calculation, the confinement factor in the gain medium of the metallo-dielectric cavity (Fig. 1(b)) is 0.39 compared to 0.19 in the pure dielectric cavity case (Fig. 1(c)). The Q factor of metallo-dielectric cavity is 726 which is a factor of 5 enhancement from the Q factor of the

#149547 - $15.00 USD Received 20 Jun 2011; revised 9 Sep 2011; accepted 30 Sep 2011; published 18 Oct 2011

dielectric cavity (Q = 151). When the gain core size is decreased below the wavelength scale, the confinement factor is significantly degraded due to the radiation loss which was studied in the micro-disk resonators [18,19]. Figure 2(a) shows the resonant mode of a pure dielectric cavity where r_{core} = 350 nm and r_{clad} = 310 nm (Δr = 40 nm) with the low index dielectric (SiO_2) coating. This structure supports WGM with M = 3 exhibiting a significant mode spreading outside the gain medium and a low confinement factor in the gain medium (0.38).

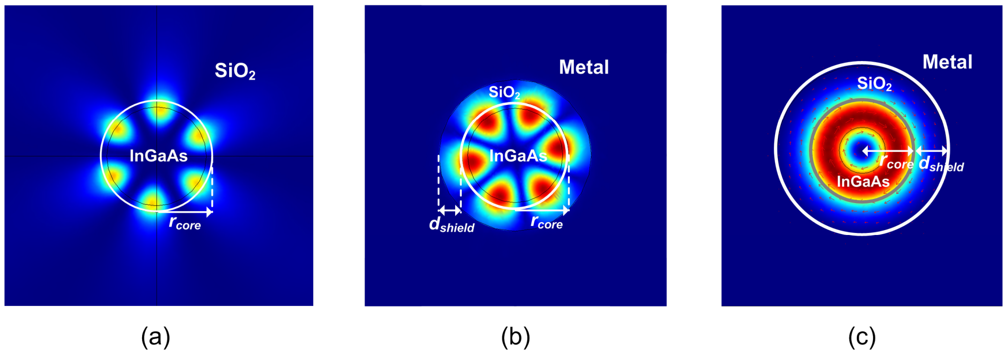

Fig. 2. The electric field intensity at the horizontal cross section of the active layer. (a) pure dielectric cavity with r_{core} = 350 nm, r_{clad} = 290 nm (Δr = 60 nm), and SiO_2 coating. (b) metallo-dielectric cavity with r_{core} = 350 nm, r_{clad} = 290 nm (Δr = 60 nm), d_{shield} = 150 nm, and Ag coating. The gain structure sizes, r_{core} and r_{clad}, in (a) and (b) are the same and the resonant mode is WGM with M = 3 for both cases. (c) metallo-dielectric cavity with r_{core} = 220 nm, r_{clad} = 160 nm, d_{shield} = 150 nm, and Ag coating. The resonant mode is axially symmetric TE_{011}.

However, by incorporation of the metallo-dielectric cavity (150 nm thick SiO_2 and Ag coating) as shown in Fig. 2(b), the resonant mode is strongly confined inside the subwavelength scale cavity and the mode overlap with the gain is also significantly enhanced. In our calculation, the confinement factor in the gain medium in metallo-dielectric cavity is 0.57. Thus for such small size resonators, this results in a factor of 22 improvement in the Q factor of metallo-dielectric cavity (Q = 468) compared to the Q factor of the pure dielectric cavity (Q = 21). Metallo-dielectric cavity enables further reduction of the gain core size while keeping efficient mode confinement in the gain medium. We numerically calculated the resonant mode of the metallo-dielectric cavity with r_{core} = 220 nm, r_{clad} = 160 nm (Δr = 60 nm) and d_{shield} = 150 nm. As shown in Fig. 2(c), for this case, the resonant mode is an axially symmetric mode (TE_{011}) for which the electric field is circulating around the gain core and is well-confined in the gain medium. The electric field intensity is mostly contained inside the gain medium with minimal mode overlap with the metal region. The Q factor of this resonator is calculated to be 707 with the threshold gain of 236 cm^{-1} which is lower than InGaAs bulk gain (400 cm^{-1}) at room temperature at 1.5 μm [20].

The pedestal geometry is adopted in our metallo-dielectric cavity pillar laser structure to enhance the optical confinement in vertical direction while keeping the pillar height less than the lasing wavelength for achieving a subwavelength scale device. To quantitatively analyze the effect of the pedestal in our laser structure, we calculated the Q factor and the threshold gain by varying r_{clad}. The calculated Q factor and threshold gain for 750 nm core radius with various r_{clad} is presented in Fig. 3(a). Shield thickness (d_{shield}) and the metal coating were kept constant. When r_{clad} is the same as r_{core} (cylinder type), the Q factor is 163 and the threshold gain is 1505 cm^{-1}. As r_{clad} is reduced to 600 nm (pedestal type, Δr = 150 nm), the Q factor is enhanced to 1731 which is about an order of magnitude improvement and the threshold gain is decreased to 99 cm^{-1} which is 93% reduction. As the pedestal undercut is made deeper (Δr is larger), the threshold gain is flattened and the resonant wavelength is shifted out of the optimal gain spectrum which is not desirable. We also calculated the Q factor and threshold gain when r_{core} = 220 nm with changing the pedestal size which is shown in Fig. 3(b). The Q factor is enhanced from 152 (cylinder type, Δr = 0 nm) to 1572 (pedestal type, Δr = 150 nm)

#149547 - $15.00 USD Received 20 Jun 2011; revised 9 Sep 2011; accepted 30 Sep 2011; published 18 Oct 2011

which is an order of magnitude improvement. The resonant mode is strongly confined inside the gain layer with pedestal structure as shown in Fig. 3(d) where r_{core} = 220 nm and Δr = 120 nm compared to the cylinder type structure shown in Fig. 3(c). The threshold gain is reduced from 1473 cm^{-1} to 89 cm^{-1} which is 94% reduction. The threshold gain of 89 cm^{-1} is a promising result for possible room temperature operation of this laser structure. As shown in both cases, the threshold gain is significantly suppressed with minimal pedestal undercut. At Δr = 60 nm, the threshold gain of 750 nm and 220 nm r_{core} are 338 cm^{-1} and 236 cm^{-1}, respectively, which are still lower than our target threshold gain of 400 cm^{-1} [20]. This is another advantage since heat dissipation and carrier diffusion in the active layer have been critical issues for most pedestal type micro-disk lasers [21,22].

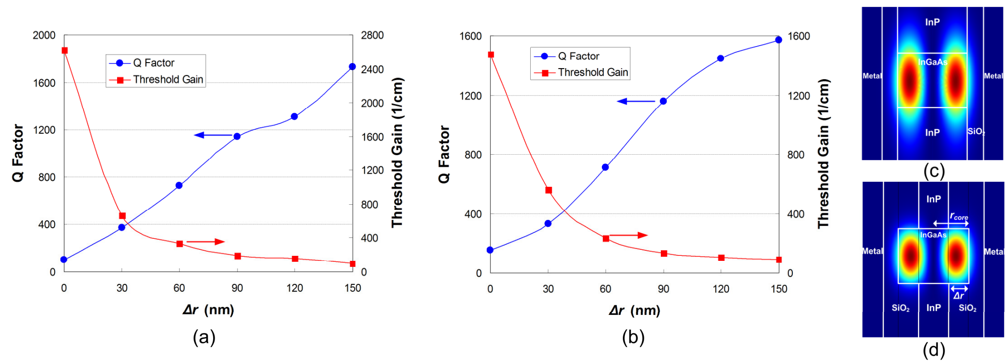

Fig. 3. Numerical simulation results of the cavity Q factor and threshold gain for various pedestal sizes. Δr (= r_{core} - r_{clad}) is pedestal undercut depth. (a) r_{core} = 750 nm, d_{shield} = 150 nm, and r_{clad} is varied from 750 nm to 600 nm (Δr = 0 ~150 nm). Blue curve represents the cavity Q and red curve for the threshold gain. (b) r_{core} = 220 nm, d_{shield} = 150 nm, and r_{clad} is varied from 220 nm to 70 nm (Δr = 0 ~150 nm). (c) Vertical cross section of the resonant mode field (TE_{011}) intensity when r_{core}, r_{clad} = 220 nm (Δr = 0 nm, cylinder type), and d_{shield} = 150 nm. (d) The resonant mode field (TE_{011}) intensity when r_{core} = 220 nm, r_{clad} = 100 nm (Δr = 120 nm, pedestal type), and d_{shield} = 150 nm.

3. Fabrication procedure

The wavelength scale (750 nm radius) and sub-wavelength scale (355 nm radius) circular masks on InGaAs/InP heterostructure wafer were patterned by the e-beam lithography on the spin-coated hydrogen silsesquioxane (HSQ) resist. Subsequent dry etching was performed using CH_4:H_2:Ar gas chemistry to form the subwavelength scale pillar structure (the scanning electron microscopy (SEM) micrograph is shown in Fig. 4(a)). The selective etching of the cladding InP layers was performed using HCl:H_3PO_4 (1:3) wet etching and the result of which is shown in Fig. 4(b). 160 nm of InP was etched on both sides through the wet etching process while the gain layer was preserved. 150 nm of SiO_2 layer was conformally deposited on the pedestal pillar surface by PECVD process which provides the low index shield minimizing the mode-metal overlap and passivates the InGaAs surface. The SiO_2 layer on the top of the subwavelength pillar structure was removed through the photoresist planarization and SiO_2 dry etching to access the n-side contact layer (n-InGaAs). Metal contacts (Ti/Pd/Au) were formed on the top of the pillar structure by the e-beam evaporation and lift-off (Fig. 4(d)). After n contact formation, a 200 nm thick silver layer was deposited to cover the whole pillar structure including the top and side wall of the pillar and n contact pad (Fig. 4(e)). A 20 nm thin Chromium (Cr) layer was deposited prior to the silver deposition for better adhesion. Since a high optical loss of Cr could degrade the Q factor of the cavity and therefore increase the threshold gain, the unintentionally deposited Cr on the side wall of the pillar structure was subsequently removed by Cr wet-etching while protecting the adhesion layer on the substrate by the photoresist masking. P-contact was separately processed by the photolithographic patterning and wet-etching of SiO_2 and InP layer to access the underlying highly doped

#149547 - $15.00 USD Received 20 Jun 2011; revised 9 Sep 2011; accepted 30 Sep 2011; published 18 Oct 2011

InGaAsP layer. The sample was then annealed to 400 °C to reduce the contact resistance. Finally, the sample was mounted on the device package (TO 8) and wire-bonded.

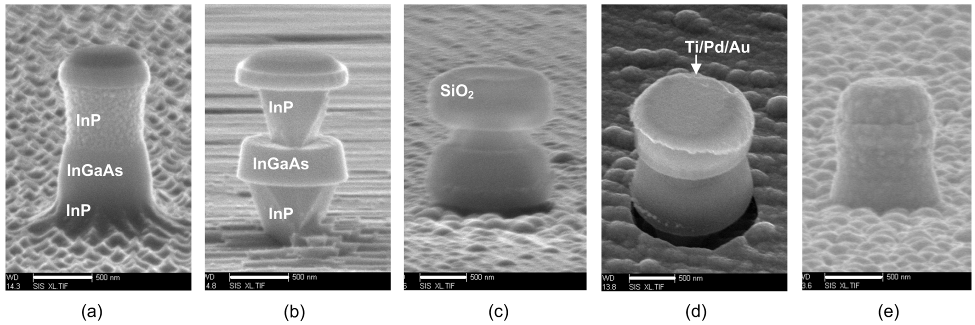

Fig. 4. SEM micrographs of subwavelength pillar laser structure during fabrication procedure. (a) Subwavelength pillar (r_{core} = 395 nm) structure after dry etching. (b) Pedestal pillar is formed by selective InP wet etching. (c) Thin SiO_2 layer (140 nm) is deposited on the pillar structure by PECVD. (d) N-contact metal (Ti/Pd/Au) layer deposited on the top of subwavelength pillar. (e) Silver is deposited on whole pillar structure. Scale bar in each image represents 500 nm.

4. Measurement and discussion

The devices were forward biased and the continuous wave (CW) emission from the device was collected through a 20 × objective lens and then imaged by the CCD camera. The spectral characteristics were analyzed by the monochromator with a maximum spectral resolution of 0.35 nm (with a 100 µm slit opening). The lasing characteristics of electrically pumped pedestal pillar lasers with two gain core radii (750 nm and 355 nm) were measured and analyzed. Figure 5(a) shows a SEM micrograph of the pedestal pillar in which r_{core} = 750 nm, r_{clad} = 710 nm with 1.3 µm pillar height. The shield thickness (d_{shield}) was 140 nm and silver was coated as a metal cavity. In the numerical simulation, the Q factor was estimated to be 458 and the threshold gain was 534 cm^{-1} at the resonant wavelength of 1.50 µm. The lasing characteristics of this device at 77 K are shown in Fig. 5(b). Electroluminescence (EL) around 1.55 µm was observed when the injected current was higher than 20 µA. As the injected current was increased, the emission spectrum showed a spectral narrowing and the lasing peak appeared at 1.49 µm which is very close to the calculated resonant wavelength of 1.50 µm. The light output-injection current (*L-I*) curve (Fig. 5(c)) shows the kink around the threshold current (50 µA) which is also an indication of the onset of lasing. The linewidth narrowed to 0.9 nm with the injection current of 300 µA. The measured Q below threshold was 271 which is 60% of the simulation result. It should be noted that the fabricated pedestal pillar (Fig. 5(a)) showed some deviations from the ideal model used in the simulation including the tapered side wall and surface roughness in InP layers which could cause this degradation of the Q factor. We also investigated the temperature dependence of the lasing characteristics of this device. A local heater inside the cryostat kept the target temperature constant during the measurement. Lasing behavior was observed at 100 K, 120 K and 140 K with constant current pump. The spectral evolution and *L-I* curve at 140 K is shown in Fig. 5(e). The lasing wavelength remains in the vicinity of 1.49 µm and the linewidth was also less than 1 nm at 140 K. However, the threshold current increased to 240 µA (inset in Fig. 5(e)) which is 5 times higher than the threshold current at 77 K. At 160 K, spectral narrowing at 1.49 µm is still observed but failed to reach lasing primarily due to the heat generation inside the cavity and the higher optical loss in metal cavity.

#149547 - $15.00 USD Received 20 Jun 2011; revised 9 Sep 2011; accepted 30 Sep 2011; published 18 Oct 2011

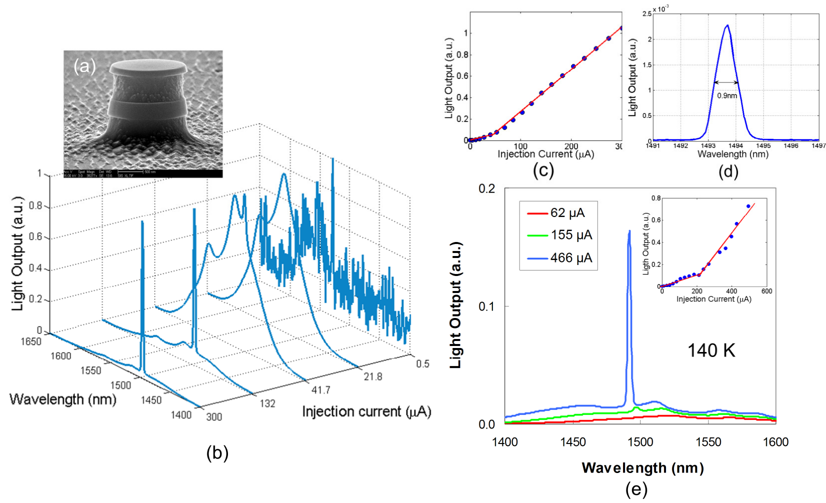

Fig. 5. Lasing characteristics of 750 nm r_{core} pedestal pillar laser device. (a) An SEM micrograph of 750 nm r_{core} pedestal pillar structure. (b) Spectral evolution graphs with increasing the injection current at 77 K. (c) *L-I* curve of this device. (d) Linewidth measurement by a monochromator with 0.35 nm resolution. (e) Lasing spectrum measured at 140 K. Inset shows *L-I* curve at 140 K.

The lasing characteristics of 355 nm core radius subwavelength pillar laser were also investigated as shown in Fig. 6. An SEM micrograph of the pedestal pillar structure is shown in Fig. 6(a). The pillar structure had r_{core} = 355 nm, r_{clad} = 310 nm, d_{shield} = 140 nm with 1.36 µm pillar height and silver coating. As discussed in the numerical simulation, this cavity structure supports the WGM with M = 3. From the simulation, the Q factor was estimated at 352 and the threshold gain was 692 cm^{-1} at the resonant wavelength of 1.38 µm. As shown in Fig. 6(b), the spectral narrowing was observed as injection current was increased and the lasing peak occurred at 1.41 µm. The threshold current was estimated around 540 µA which is 10 times higher than for the 750 nm r_{core} device due to the lower material gain at shorter wavelengths and higher threshold gain. The resonant wavelength from the simulation (1.38 µm) matches the measurement results quite well. Higher resolution analysis of the lasing peak spectrum showed that the lasing peak at 1.41 µm is a dual peak with 1.5 nm splitting (Fig. 6(d)), which indicates the imperfect circular symmetry of the pillar structure due to fabrication. When the temperature is increased, the CW lasing operation was observed up to 100 K. As shown in Fig. 6(e), the onset of the lasing peak is clearly observed and the linewidth is about 6 nm at 100 K. At 120 K, the output spectrum showed clear spectral narrowing with 8 nm linewidth which indicates the cavity mode, but failed to reach lasing which could be due to the heating from the high driving current. It is expected that pulsed operation could reduce the heating issue so that the device could operate at even higher temperatures. Based on our numerical simulation above, a smaller size (r_{core} = 220 nm) device should be able to be lase with a low threshold gain (< 100 cm^{-1}). However, the fabrication difficulties such as forming pedestal structure on 200 nm width InP cladding with the wet etching process are still challenging and the thermal management becomes even more critical with subwavelength scale pillar widths. We are currently working on resolving these issues by optimizing our fabrication process and developing a low resistance contact design which could reduce the electrical power dissipation and self-heating in the device. Incorporation of quantum well or quantum dot gain structures in our laser devices could also allow for building highly efficient subwavelength-scale lasers [11,23].

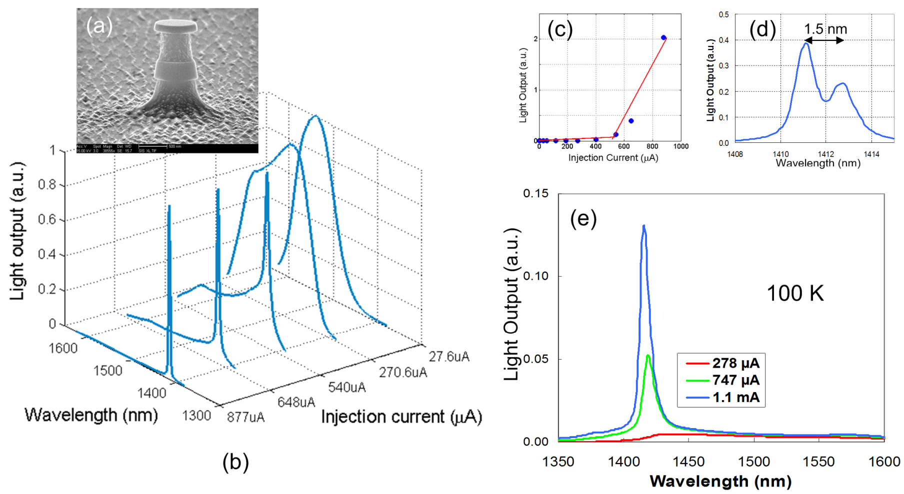

Fig. 6. Lasing characteristics of 355 nm r_{core} pedestal pillar laser device. (a) An SEM micrograph of 355 nm r_{core} pedestal pillar structure. (b) Spectral evolution graphs with increasing the injection current at 77 K. (c) *L-I* curve of this device. (d) Linewidth measurement by a monochromator. (e) Lasing spectrum with difference injection currents measured at 100 K.

5. Conclusion

We demonstrated a new design and fabrication wavelength and sub-wavelength scale electrically driven lasers using metallo-dielectric cavities. In the design, the metal cavity combined with thin low index dielectric layer enabled a significant enhancement in mode confinement for both wavelength and subwavelength scale cavities. Using a pedestal geometry improved the vertical mode confinement and showed a huge reduction in the threshold gain with increasing undercut in pedestal cladding. To lower the threshold gain below the target 400 cm^{-1}, it requires a minimal undercut (< 60 nm) in the pedestal for 750 nm and 350 nm core radius laser. This is a clear advantage for efficient heat transfer and carrier diffusion in the active region. In the experiment, we presented the fabrication process for our designed structure based on InGaAs/InP double heterostructure. Laser devices were fabricated for 750 nm and 355 nm gain core radii. We observed a clear lasing operation at 77 K for both laser devices with low threshold current of 50 μA and 540 μA, respectively. For the r_{core} = 750 nm laser device, the CW lasing operation at 1.49 μm was observed up to 140 K. The r_{core} = 355 nm laser device showed the CW lasing operation up to 100 K. Numerical studies suggest that even smaller laser structures (core radius = 220 nm) could exhibit low threshold gain which is also feasible for room temperature operation.

Acknowledgments

Authors would like to acknowledge the support from the Defense Advanced Research Projects Agency (DARPA) under the NACHOS program, the National Science Foundation (NSF), the NSF's Engineering Research Center for Integrated Access Networks (CIAN), the Cymer Corporation and the U.S. Army Research Office. The fabrication was performed at UCSD Nano3 facilities.